Nonlin. Processes Geophys. Discuss., 1, 1621–1655, 2014
www.nonlin-processes-geophys-discuss.net/1/1621/2014/
doi:10.5194/npgd-1-1621-2014


Nonlinear Processes in Geophysics
Discussions
Open Access



# Temperature distribution and Hadley circulation in an axisymmetric model

**N. Tartaglione**

School of Science and Technology, University of Camerino, Camerino, Italy

Received: 5 October 2014 – Accepted: 7 October 2014 – Published: 3 November 2014

Correspondence to: N. Tartaglione (nazario.tartaglione@unicam.it)

Published by Copernicus Publications on behalf of the European Geosciences Union & the American Geophysical Union.







## Abstract

The impact of the temperature distribution on the Hadley circulation simulated by an axisymmetric model is studied. The temperature distributions that drive the model are modulated here by two parameters, $n$ and $k$, the former controlling the horizontal broadness and the latter defining change in the vertical lapse rate. In the present study, the changes of the temperature distribution mimic changes of the energy input of the atmospheric system leaving as an invariant the equator-poles difference. Both equinoctial and time-dependent Hadley circulations are simulated and results compared. The results give evidence that concentrated temperature distributions enhance the meridional circulation and jet wind speed intensities even with a lower energy input. The meridional circulation and the subtropical jet stream widths are controlled by the broadness of horizontal temperature rather than the vertical lapse rate $k$, which is important only when the temperature distribution is concentrated at the equator. The jet stream position does not show any dependence with $n$ and $k$, except when the temperature distribution is very wide and in such a case the jet is located at the mid-latitude. Using $n = 2$ and $k = 1$ we have the formulation of the potential temperature adopted in classical literature. A comparison with other works is performed and our results show that the model running in different configurations (equinoctial, solstitial and time-dependent) yields results similar to one another.

## 1 Introduction

The earth's atmosphere is driven by differential heating of the earth's surface. At the equator, where the heating is larger than that at other latitudes, air rises and diverges poleward in the upper troposphere, descending more or less at 30° latitude (subtropics). This circulation is known as Hadley cell. Because of the earth's rotation, this circulation produces two subtropical jets. A poleward shift (Fu and Lin, 2011) and an enhanced wind speed of these jets (Strong and Davis, 2007) are associated with a





NPGD
1, 1621–1655, 2014



possible Hadley cell widening and strengthening, which has been observed in the last decades (Fu et al., 2006; Hu and Fu, 2007; Seidel et al., 2008; Johanson and Fu, 2009; Nguyen et al., 2013).

There are a few studies suggesting possible causes of these phenomena. One of the theories postulates global warming as a possible cause of Hadley cell widening (Lu et al., 2009). However, the atmosphere is a complex system containing many subsystems interacting with one another and the global warming might not be the only cause that is suggested to explain the widening. Ozone depletion (Lu et al., 2009; Polvani et al., 2011), SST warming (Staten et al., 2011) and aerosol (Allen et al., 2012) have been invoked to explain the Hadley cell widening.

Climate models vary to some extent in their response and the relationship between global warming and Hadley cell is not straightforward. For instance, Lu et al. (2007) found a smaller widening than the observed one. Gitelman et al. (1997) showed that the meridional temperature gradient decreases with increasing global mean temperature and the same result can be found in recent modeling studies (Schaller et al., 2013).

Much of our understanding on the Hadley cell comes from theories using simple models (Schneider, 1977; Schneider and Lindzen, 1977; Held and Hou, 1980, hereafter HH80) and such a simple model will be adopted here in order to understand how temperature distributions can change the Hadley circulation. How much temperature change impacts the real Hadley circulation is not clear yet, perhaps because of discrepancies between observations, reanalysis (Weliser et al., 1999) and climate model outputs, although these differences are becoming less marked because of newer observational datasets or correction of the older ones (Sherwood, 2008; Titchner et al., 2008; Santer et al., 2008). Hence, it is critical to understand the possible mechanisms behind the cell expansion starting from a simple model.

The objective of this study is to analyze the sensitivity of a model of the symmetric circulation to the radiative-convective equilibrium temperature distribution. Our point of departure is the symmetric model used by Cessi (1998), which is a bidimensional model considering atmosphere as a thin spherical shell. This model will be briefly





NPGD
1, 1621–1655, 2014



described in Sect. 2. The model describes mainly a tropical atmosphere, hence it does not allow for eddies. Although eddies may play a central role in controlling the strength and width of the Hadley cell (e.g. Kim and Lee, 2001; Walker and Schneider, 2006), a symmetric circulation, driven by latitudinal differential heating, can exist even without eddies and it is a robust feature of the atmospheric system (Dima and Wallace, 2003). The temperature distributions used in this study represent some paradigms of tropical atmospheres. Among the possible causes that can change temperature distributions there are El Niño, global warming and change of solar activity. We will show, in Sect. 3, that the energy input is not as important as the temperature distribution. Our results are consistent with those obtained both by Hou and Lindzen (1992) (hereafter HL92), and recently by Tandon et al. (2013) who performed experiments similar to those described here. The conclusions will be drawn in Sect. 4.

## 2 The model

The model used in this study is a bidimensional model of the axis-symmetric atmospheric circulation described in Cessi (1998). The horizontal variable is defined as $y = a\sin\phi$ from which we have

$$c(y) = \cos\phi = \sqrt{(1 - y^2/a^2)} \tag{1}$$

where $a$ is the radius of a planet having a rotation rate $\Omega$, the height of atmosphere is prescribed to be $H$.

The model is similar to the Held and Hou model (HH80), but the difference is that, the model prescribes a horizontal diffusion $\nu_H$ other than the vertical diffusion $\nu_v$. The prognostic variables are the angular momentum $M$, defined as $M = \Omega a c^2 + uc$ where $u$ represents the zonal velocity; the zonal vorticity $\psi_{zz}$ with the meridional stream function $\psi$ defined by





NPGD
1, 1621–1655, 2014



$$\partial_y \psi \equiv w;$$
$$\partial_z \psi \equiv -cv \tag{2}$$

and the potential temperature $\theta$ that is forced towards a radiative-convective equilibrium temperature $\theta_E$. Starting from the dimensional equations of the angular momentum, zonal vorticity and potential temperature, we will obtain a set of dimensionless equations. The new equations are non-dimensionalized using a scaling that follows Schneider and Lindzen (1977), but the zonal velocity u is scaled with $\Omega a$. A detailed description can be found in Cessi (1998).

The non-dimensional model equations are:

$$M_t = \frac{1}{R}\left\{M_{zz} + \mu\left[c^4(c^{-2}M)_y\right]_y\right\} - J(\psi, M) \tag{3a}$$

$$\psi_{zzt} = \frac{1}{(R^2E^2)} y c^{-2}(M^2)_z - \frac{1}{c^{-2}} J(\psi, c^{-2}\psi_{zz}) + \frac{1}{(RE^2c^{-2})}\theta_y + \frac{1}{(Rc^{-2})}\left[c^{-2}\psi_{zzzz} + \mu\psi_{zzyy}\right] \tag{3b}$$

$$\theta_t = \frac{1}{R}\left\{\theta_{zz} + \mu\left[c^2\theta_y\right]_y + \alpha[\theta_E(y,z) - \theta]\right\} - J(\psi, \theta). \tag{3c}$$

The term $J(A,B) = A_yB_z - A_zB_y$ is the Jacobian.

The thermal Rossby number $R$; the Ekman number $E$, the ratio of the horizontal to the vertical viscosity $\mu$ and the parameter $\alpha$ are defined as

$$R \equiv gH\Delta_H/(\Omega^2a^2); \quad E \equiv \nu_V/(\Omega H^2); \quad \mu \equiv (H^2/a^2)\nu_H/\nu_V; \quad \alpha \equiv H^2/(\tau\nu_V). \tag{4}$$

The term $\alpha$ is the ratio of the viscous timescale across the depth of the model atmosphere to the relaxation time $\tau$ toward the radiative-convective equilibrium.





NPGD
1, 1621–1655, 2014



The boundary conditions for the set of Eq. (3) are:

$$
\begin{aligned}
&M_z = \gamma(M - c^2), \quad \psi_{zz} = \gamma\psi_z;\\
&\psi = \theta_z = 0 \quad \text{at} \quad z = 0;\\
&M_z = \psi_{zz} = \psi = \theta_z = 0 \quad \text{at} \quad z = 1
\end{aligned}
\tag{5}
$$

where $\gamma = \frac{CH}{\nu_V}$ is the ratio of the spin-down time due to the drag to the viscous timescale, the bottom drag relaxes the angular momentum $M$ to the local planetary value $\Omega a c^2$ through a drag coefficient $C$.

The model flow started from an isothermal state at rest and is maintained by a Newton heating function where the heating rate is proportional to the difference between the model potential temperature and a specified radiative-convective equilibrium temperature distribution, which follows the HH80 one:

$$\theta_E = \frac{4}{3} - y^2 + \frac{\Delta_V}{\Delta_H}\left(z - \frac{1}{2}\right). \tag{6}$$

We will assume that Eq. (6) is the radiative-convective equilibrium temperature distribution of the control experiment; we define a general form of the Eq. (6) as

$$\theta_E = \frac{4}{3} - |y|^n + \frac{\Delta_V}{\Delta_H}\left(z^k - \frac{1}{2}\right). \tag{7}$$

The values $n$ and $k$ control the horizontal homogenization of the temperature and the lapse rate respectively. When $n = 2$ and $k = 1$ Eq. (7) becomes the reference equilibrium temperature given in Eq. (6). In many other works (e.g. Schneider, 1977; HH80; Caballero et al., 2008), the considered atmosphere is essentially dry; however the distribution of temperature of a dry atmosphere can reflect an action of the water vapor condensation (HL92). Tandon et al. (2013) used narrow and wide thermal forcing to mimic El Niño or global warming effect on a tropical circulation in a Global Circulation Model.





NPGD
1, 1621–1655, 2014



Starting from Eq. (7) a set of experiments were performed changing $n$ and $k$ in such a way to have a set of numerical results. In order to isolate the contribution of the temperature distribution on the solution of Eq. (3), a set of parameters will be used:

$$
\begin{aligned}
&a = 6.4 \times 10^6\,\mathrm{m} && \Omega = 2\pi/(8.64 \times 10^4)\,\mathrm{s}^{-1} \\
&\Delta_H = 1/3 && \Delta_V = 1/8 \\
&g = 9.8\,\mathrm{m\,s}^{-2} && C = 0.005\,\mathrm{m\,s}^{-1} \\
&H = 8 \times 10^3\,\mathrm{m} && \tau = 20\,\mathrm{days} \\
&\nu_V = 5\,\mathrm{m}^2\,\mathrm{s}^{-1} && \nu_H = 1.86\,\mathrm{m}^2\mathrm{s}^{-1}.
\end{aligned} \tag{8}
$$

The parameters in Eq. (8) are the same as those used by Cessi (1998).

The meridional and vertical gradients are controlled by the parameters $n$ and $k$, where they vary from 0.5 to 3 with a 0.5 step, in such a way that we have a set of 36 simulations. The average temperature along the latitudes and heights are shown in Fig. 1. Heating functions with $n$ value equal to 0.5 should not be regarded as unreal, but merely as a simple way to represent a specific state of the atmosphere. The same assertion is valid for all other parameters. As $n$ increases the average temperature increases as well, but the meridional gradient decreases. High $n$ values represent situations with a model atmosphere temperature homogenized along the meridional direction (Fig. 1a).

With the prescribed temperature as stated in Eq. (7), the temperature at the boundaries and its equator-pole difference remain invariant with respect to $n$ and $k$. The mean temperature is not constant here, which differs from HL92, which analyzed the influence of concentration heating perturbing the forcing function $\theta_E(y,z)$ in such a way that its average over the domain remained constant. It is easily visible in Fig. 1b. Higher $n$ values, keeping $k$ invariant, have higher mean temperatures at all levels. The same is true for $k$, with higher $k$ values, for $n$ constant, the mean temperature for each level is always higher than that with lower $k$ values. The pole-equator temperature difference at upper and lower vertical boundaries are the same for all the experiments, but





NPGD
1, 1621–1655, 2014



the meridional (vertical) temperature gradient changes as a function of $n(k)$. Whether global warming makes the earth temperature distribution narrower or wider is beyond the aim of the paper. One can expect that global warming broadens the temperature distribution, but at the same time it could have an impact above all on the SST bringing more water in the upper atmosphere which changes the vertical distribution of the temperature in the intertropical convergence zone. Since other causes can change the temperature distribution of a planet such as changes in the solar activity for instance, we will focus on the temperature distribution regardless of its cause.

Although in this model the atmosphere is dry, changing the temperature distribution allows for a change in the static stability. Looking at the mean temperature along the vertical direction, low values of $k$ are related to low values of static stability, especially in higher level of the model atmosphere.

The Brunt–Väisälä frequency $N^2 = g\frac{\theta_z}{\theta}$, when the atmosphere reaches the equilibrium will be

$$N^2 = \frac{\left(gk\Delta_V/\Delta_H z^{(k-1)}\right)}{\left[4/3 - y^n + \Delta_V/\Delta_H\left(z^k - 1/2\right)\right]}. \quad (9)$$

It is clear from Eq. (9) that the Brunt–Väisälä frequency does not depend on $n$ at the poles and equator. On the contrary, large values of $k$ imply a more stable atmosphere in the upper levels, especially at poles, making the model atmosphere more similar to the real one, simulating in some respects a sort of tropopause. Moreover, this is equivalent to creating a physical sponge layer in the upper levels of the model that will have some effects on the vertical position of stream function maximum.

## 3 Numerical results

This section is divided into three subsections, the first showing the results of the model applying the equinoctial condition, when the sun is assumed to be over the equator.





NPGD
1, 1621–1655, 2014



The solution is steady as already shown for instance in Cessi (1998). The second subsection will show the results of the model having a temperature distribution described by Eq. (7) but moving following a seasonal cycle. The case $n = 2$ and $k = 1$ is discussed in the third subsection in comparison with previous studies.

### 3.1 Equinoctial conditions

The axially symmetric circulation is forced by axially symmetric heating as in HH80 and many others and as prescribed by Eq. (7). The model started from an isothermal state and it was run for 300 days, even though it reached its equilibrium approximately after 100 days, in order to be sure that the model does not have instabilities in the long run.

The absolute value of the maximum stream function intensity at the equilibrium conditions for the 36 experiments is shown in Fig. 2. When $n = 0.5$, with $k$ constant, the circulation is always the strongest. The stream function intensity is inversely proportional to $n$ (Fig. 2a). With $n = 0.5$ the experiment resembles the one described in HL92 where they concentrated the latitudinal extent of heating and this led to a more intense circulation. However, they imposed the forcing function $\theta_E(x, y)$ in such a way that its average over the domain remained the same as in the control experiment, i.e. without changing the energy input. They found that concentration of the heating through a redistribution of heat within the Hadley cell led to a more intense circulation without altering its meridional extent. Instead, here, it is evident from Fig. 1 that the experiment with $n = 0.5$ has an energy input lower than the other cases. Nevertheless, the Hadley circulation is always more intense than the other cases and contrary to higher $n$ value experiments, the circulation is confined close to the equator. Thus the results of HL92 are extended to a more general case with a lower energy input. It is worth noting the constraint of an equal pole-equator gradient of mean temperature is assumed here which is different from HL92 (Fig. 1a).

The dependence on $k$ is not as straightforward as the one on $n$, instead. The stream function reaches the highest value for $k = 3$. With a high $n$ values the Hadley cell stream function intensity is lower and the dependence on $k$ loses its importance. In other





NPGD
1, 1621–1655, 2014



words, in our model, the symmetric circulation strength is modulated by $k$ only when the temperature distribution is concentrated to the equator.

Figure 2b shows the maximum zonal wind speed as function of $n$ and $k$, it is inversely proportional to $n$, the dependence on $k$ is not as clear as the one on $n$ and when $n = 3$ it almost vanishes in accordance with the behavior of the maximum stream function. These results are in agreement with HL92, who found a stronger zonal wind when the temperature was concentrated at the equator.

Some studies define the border of a Hadley cell as that by the zero line of the 500 hPa stream function (e.g. Frierson et al., 2007). Since the circulation intensity changes greatly in our experiments, it is problematic to define a width of the Hadley cell based on the absolute value of the circulation itself. Moreover the stream function goes to zero in the model only at the poles. Hence, we will define the position of the cell equal to the position of the maximum value of stream function, in this way we will study a possible poleward shift of the cell as a function of the two parameters $n$ and $k$. The width of the cell will be defined more or less by isolines having 1/4 of the maximum value of the stream function. It is worth noting that this definition is an operational one and does not resemble the definition used by Dima and Wallance (2003) or Frierson et al. (2007).

The latitude of the maximum stream function value shows a general dependence on $n$ and $k$. It increases with $n$ and decreases with $k$. However, as shown in Fig. 3a, this dependence is not straightforward or linear, although we have a few exceptions, for instance when $k = n = 0.5$. Hence in general when $n$ increases, and the total energy input is larger, the stream function is weaker but poleward. This is in contrast with the recent observations where a slight strengthening and widening of the Hadley Circulation for the past three decades was observed by Liu et al. (2012) and a poleward expansion was also found by Hu and Fu (2007). However, Liu et al. (2012) showed that if the observations start from 1870, the Hadley cell becomes more narrow and stronger.

The height of the maximum stream function value is confined for almost all the simulations under 2200 m and the general rule is that when $n$ increases, the height of maximum lowers, however a few experiments, those with $k = 0.5$ and $n = 0.5$, 1 and





NPGD
1, 1621–1655, 2014



1.5, have the maximum value between 4300 and 5600 m exhibiting an increase in the height with $n$ (Fig. 3b).

In general, the location of the maximum zonal wind speed does not show any evident relationship with the parameters $n$ and $k$. It is always confined between 26 and 29° off the equator; however when $n = 3$, there is an abrupt transition to about 48°, independently from the $k$ value. In Table 1, we show the latitude of the maximum wind speed when $k = 1$ for different $n$ values.

It is worth calculating the prediction of the cell edge following the HH80 assumptions. HH80 showed that the Hadley cell has a finite width with the edge ending at a specific latitude $\varphi_H$ and calculated a scaling for this latitude. Starting with the vertically integrated hydrostatic equation and a balanced zonal wind, HH80 obtained a formulation for $\theta$ in the limit inviscid:

$$\bar{\theta}(\phi) = \bar{\theta}(0) - \bar{\theta}_0 \frac{\omega^2 a^2 \sin^4(\phi)}{2gH\cos^2(\phi)}. \tag{10}$$

Assuming continuity of the potential temperature $\bar{\theta}(\phi_H) = \bar{\theta}_E(\phi_H)$ and conservation of vertically averaged potential temperature $\int_0^{\phi_H} \bar{\theta}\cos(\phi)\mathrm{d}\phi = \int_0^{\phi_H} \bar{\theta}_E\cos(\phi)\mathrm{d}\phi$, they found $\varphi_H$ as a function of the Rossby number $R$. The hypothesis of continuity and conservation of potential temperature is equivalent to solving those two equations by means of a geometric "equal-area" construction.

For the general case described by Eq. (7), we calculated a similar relationship between $\varphi_H$ and the Rossby number, assuming the same hypothesis of HH80 described previously.

$$R = \left[\frac{(n+1)}{2n}\right] \frac{\left[\left(y_H^5/(1-y) + y_H + 1/3y_H^3 - 1/2\ln\left((1+y_H)/(1-y_H)\right)\right)\right]}{y_H^{(n+1)}} \tag{11}$$

The $n$ value goes from 0.5 to 3. Eq. (11) should be compared with Eq. (17) of HH80. We represent the solutions of Eq. (11) in Fig. 4. Evidently for $R = 0.121$ (that is the Rossby





NPGD
1, 1621–1655, 2014



number used here), there is no agreement when $n = 3$ between analytic solution that predicts a smaller $\varphi_H$ and the numerical one, which differs from all the other solutions that are quite close to one another.

This behavior could be related to the diffusivity. Figure 5 shows the analytic and numerical vertically averaged potential temperature for $n = k = 3$. It is evident that not only $\bar{\theta}$ is not conserved when $n = 3$ and there is not redistribution of energy, hence the assumption made by HH80 about the continuity and conservation of potential energy and that leads to Eq. (11) never takes place in the numerical model for $n = 3$. However, when the vertical diffusion is very small or $k$ has low values $\bar{\theta}$ approaches to $\bar{\theta}_E$ (not shown) but the jet streams have their maxima at the mid-latitudes.

Figure 6 shows the stream function and the zonal wind speed for the experiments $n = k = 0.5$ (Fig. 6a) and $n = k = 3$ (Fig. 6b). The parameter $n$ controls the Hadley cell and jet stream widths. The experiment with $n = k = 0.5$ has Hadley cells and jet streams quite narrow. As far as the vertical position of the maximum value of the stream function is concerned, the experiments with $k = 0.5$, 1 and 1.5 exhibit particular behavior with respect to the other experiments. The stream function has its maximum at upper levels. It is likely that such a combination of the parameters favors air to move to higher levels with respect to experiments with higher $k$ values.

HH80 found that the edge of the Hadley cell was at the mid-latitudes when the planetary rotation was lower than that of the earth. Since this phenomenon is here observed for a wider temperature distribution, this common result may be attributed to a low efficiency in the process of homogenization of momentum and temperature.

### 3.2 Time-dependent simulations

Since heating depends on solar irradiation, it is of interest to analyze the solutions obtained by the annually periodic thermal forcing and to compare it with the steady solutions described previously in this paper. Starting from Eq. (7), we can formulate a temperature distribution having the maximum heating off the equator at latitude $y_0$:





NPGD
1, 1621–1655, 2014



$$\theta_E = \frac{4}{3} - |y - y_0|^n + \frac{\Delta_V}{\Delta_H}\left(z^k - \frac{1}{2}\right) \quad (12)$$

where $y_0$ in Eq. (9) is dependent on time according to

$$y_0(t) = \sin\left(\frac{\varphi_0 \pi}{180}\right) \cdot \sin\left(\frac{2\pi t}{360\,\mathrm{d}}\right) \quad (13)$$

where $\varphi_0$ is the maximum latitude off the equator where heating is maximum. Equations (12) and (13) are the same used by Fang and Tung (1999) with the choice of maximum extension of $\varphi_0$ consistent with the choice of Lindzen and Hou (1988), i.e. $\varphi_0 = 6^\circ$. A prescribed equilibrium temperature varying seasonally makes the simulations more realistic. As described previously, here we will focus on the average and maximum values, in absolute terms, of the stream function and zonal speed obtained during 360 days of simulations. The averaged values are obtained in these cases by averaging the outputs obtained every 30 days, starting from the minimum corresponding to the summer Hadley cell in the boreal hemisphere.

The annual averages of the time-dependent and equinoctial circulations shows that maximum stream function s and zonal wind speeds behave quite similarly in the annual averages of the time-dependent and equinoctial circulations. Nevertheless the time-dependent solutions never attain the symmetric circulation obtained by averaging the single snapshots (Fig. 7). Even the real earth circulation never reaches the mean Hadley circulation, even because of eddies, but symmetric Hadley cells are visible in the average circulation (Dima and Wallace, 2003).

The maximum stream function is obtained here by the $k = n = 0.5$ (Fig. 7a). In general, for $k = 0.5$, we have stronger circulations and winds. It has confirmed the tendency to a weaker stream function and wind speed when $n$ increases. However, the circulation strength expressed as averaged value is weaker in the time-dependent solution, when $n$ is low and $k$ is high, otherwise it is stronger, but it is never twice as strong as that of the equinoctial solution as found by Fang and Tung (1999). When $n = 2$ and





NPGD
1, 1621–1655, 2014



$k = 1$ it appears more consistent with the results of Walker and Schneider (2005) as discussed in the Sect. 3.3. The maximum zonal wind speed shows a behavior slightly different from the stream function intensity; there is a clear dependence on $n$ and $k$. For example, there is not an analog maximum when $n = 0.5$ and $k = 3$ found in the steady solution and thus for other $k$ values where the stream function has a relative maximum. With high $k$ value the static stability is high and the maximum of circulation confined to lower levels prevents air upwelling at the high levels. Thus, the transfer of momentum to high level is less effective with respect to the case $k = 0.5$ where it is favored instead.

The meridional position of the stream function maximum shows that there is no clear dependency on $n$ and $k$ (Fig. 8). The difference between the time-dependent simulations and the average of the non-time-dependent simulations is quite interesting. It is to be noticed that the latitude of the stream function maximum in the time-dependent solution is in the range of 12.5 and 16° (Fig. 8a), whereas in the equinoctial solutions the correspondent latitude is within a larger range. It is probable that this narrow interval is due to the averaging operation. The maximum stream function is located at higher levels, between 4500 and 6000 for $n$ less than 2.5. Otherwise the maximum is positioned under 2500 m except when $n = 3$ and $k = 0.5$ (Fig. 8b).

More than the steady solution, it is evident that the height of the maximum stream function is lower when $k = 3$. In the steady solution this phenomenon is not that evident. When $k = 3$, the vertical gradient of the potential temperature is higher in upper levels and it prevents, evidently more than the equinoctial solution, air from moving higher leaving circulation occurring at lower levels. The case $k = 3$ is equivalent to imposing a "natural" sponge layer at the top of the model. Thus it does not come as a surprise that the maximum stream function is lower than those observed in simulations with other $k$ values. This result is analogous to that of Walker and Schneider (2005) that removed the maximum stream function at higher levels found by Lindzen and Hou (1988) adopting a numerical sponge layer at the top of the model. A comparison with previous works of the simulations with $n = 2$ and $k = 1$ will be discussed in the Sect. 3.3.





NPGD
1, 1621–1655, 2014



The position of the jet stream is almost similar to the one observed in the steady solution. It is confined between 28 and 30°, with latitude of averaged jet remaining almost at the same place or moving equatorward with $n$, except when $n = 3$ the jets are located at about 44° confirming the abrupt transition of the jet stream position when $n = 3$ already found for the equinoctial experiment. Fu and Lin (2011) suggest that the jets moved poleward of about 1° per decade in the last several years but Strong and Davis (2007) observed that Northern Hemisphere subtropical jet shifted poleward over the east Pacific, while an equatorward shift of the subtropical jet was found over the Atlantic basin. Excluding the case $n = 3$, all the other subtropical jets in the different experiments have the position of the maximum very close to one another and the shifting range is very limited. However, when we use the jet latitude to define the edge of the Hadley cell, there is no significant shift but when $n = 3$. This appears to be in contrast with the Held and Hou model. Both Tandon et al. (2013) and Kang and Polvani (2011) found a discrepancy in this area with the jets that do not follow the Hadley cell edge.

Figure 9 shows the annually averaged circulation for the same cases as shown in Fig. 6, which is obtained by annually averaged heating. It is impressive how the steady and time-dependent solutions resemble each other. As in Fang and Tung (1999) the annual mean meridional circulation has the same extent, but differently from them the strength of the annual mean circulation of the time-dependent solution is almost the same of the steady solution.

When the heating center is off the equator the intensity of the winter cell is stronger, whereas the cell of the summer hemisphere is weak and sometimes almost absent. Figures 10 and 11 show the maxima of the stream function and zonal wind speed at the winter solstitial as a function of $n$ and $k$. The maximum stream function as a function of $n$ and $k$ has the same configuration of the steady solution. Here, as expected the intensity of the meridional circulation (Fig. 10a) is twice as strong as that of the steady solution. The zonal wind has a different configuration instead, the maximum zonal wind is obtained when $n = 1$ (Fig. 11).





NPGD
1, 1621–1655, 2014



We can inspect a couple of simulations when the stream function reaches its maximum in the boreal hemisphere. Figure 12 shows the stream function and the zonal wind speed when $n = 2$ and $k = 0.5$ (Fig. 12a) and $n = 2$ and $k = 3$ (Fig. 12 b). When $k = 0.5$ (upper panels) the boreal (winter) circulation is much stronger when $k = 0.5$, with the austral (summer) circulation almost absent. The vertical extent is larger and the maximum is located at higher levels. The summer and winter jets are both more intense than their counterparts for $k = 3$. The tropical easterly winds are in this case stronger than those for $k = 3$ ($13.8\,\mathrm{ms}^{-1}$ vs. $11.4\,\mathrm{ms}^{-1}$) and the easterly region is also wider. When $k = 3$, it is noted that the boreal cell is located closer to the equator than the austral cell (not easily visible in the figure when $k = 0.5$).

### 3.3 A discussion on the case $n = 2$ $k = 1$

When $n = 2$ and $k = 1$, corresponding to the classic case discussed in many studies, we found that the time-dependent solution is only slightly stronger than the steady solution. Lindzen and Hou (1988) proposed a study of the Hadley circulation in which the maximum heating was 6° off the equator. In their non-time-dependent model, the solution showed an average circulation much stronger by a factor 15 for $\phi_0 = 6^\circ$ with respect to the equinoctial solution. Lindzen and Hou (1988) suggested that this exceptional strength was due to a nonlinear amplification of the annually averaged response to seasonally varying heating, although Dima and Wallace (2003) in a study on the seasonality of the Hadley circulation did not observe any nonlinear amplification.

With the parameters used for equinoctial and time-dependent simulations we performed an experiment like that of Lindzen and Hou (1988), with $\phi_0 = 6^\circ$ that will be referred to as solstitial experiment. We found that the winter circulation is stronger by a factor three with respect to the steady solution obtained with the equinoctial heating consistent with the result of the axisymmetric model in Walker and Schneider (2005). However, the average circulation, obtained by averaging two solstitial with $\phi_0 = 6^\circ$ and $\phi_0 = -6^\circ$, is only 1.5 times stronger than the steady solution with $\phi_0 = 0^\circ$ and it has a maximum in the upper levels of the model domain as in Lindzen and Hou (1988).





NPGD
1, 1621–1655, 2014



We suggest that this maximum is due to a numerical effect caused by averaging the single solstitial experiments rather than a spurious effect caused by the rigid lid as suggested in Walker and Schneider (2005), even though a sponge layer actually lowers this maximum stream function height and we can see the effects of a stronger vertical gradient in the upper levels especially in the time-dependent solution (cf. Figs. 3 and 9). Single solstitial experiments did not show a maximum in upper levels and so the equinoctial and time-dependent experiments (Fig. 13). Consequently the only operation performed to produce Fig. 13c was to average the two solstitial experiments, which causes the maximum at upper levels.

Finally, we notice that comparing a time-dependent solution with $\varphi_0 = 6^\circ$ with the equivalent steady solution having the heating off the equator is not properly correct, since for the time-dependent model $\varphi_0$ represents only the maximum extension of heating, hence a more correct comparison between time and no time-dependent solutions should be performed with the time-dependent solution having $\varphi_0 = 3^\circ$. In such a case, the average solution is only slightly weaker than the Hadley circulation driven by annually averaged heating or by a time-dependent heating which does not show any maximum in the upper levels. Thus, the results of equinoctial, time-dependent and solstitial ($\varphi_0 = 3^\circ$) experiments are mutually consistent.

## 4 Conclusions

The temperature distribution of an Earth-like planet can change for several reasons. For instance, a change of the temperature distribution can be caused by different factors such as global warming or long-term variation of solar activity.

Under the assumption of an equal equator-pole difference we used an axisymmetric model to study the sensitivity of the tropical atmosphere to different temperature distributions modulated by two parameters, $n$ that controls the broadness of the distribution and $k$ that modulates how the temperature is distributed vertically. Equinoctial and time-dependent solutions were simulated and compared. Moreover for the case $n = 2$





NPGD
1, 1621–1655, 2014



and $k = 1$, corresponding to the classical distribution used in literature, a few solstitial experiments were also run. When $n = 2$ and $k = 1$, the annually averaged circulation of equinoctial, time-dependent and solstitial experiments are quite close to one another, consistent with the results of Walker and Schneider (2006). However, the results differ from those of Lindzen and Hou (1988) and Fang and Tung (1999). As in all those works the maximum of the stream function of the solstitial experiment appears to be at upper levels, but it seems to be related to a spurious effect of the averaging operation rather than a spurious effect due to the rigid lid.

The results provide evidence that concentrated temperature distributions enhance the meridional circulation and jet wind speed intensities, confirming findings of Lindzen and Hou (1988) even though these authors imposed the same energy input. However, in the present study the concentrated distribution at the equator has lower energy input.

The width of the Hadley cell is proportional to $n$, but when the cell width increases its intensity decreases. The equator-pole gradient is the same for all the experiments; hence it is the gradient equator-subtropic that controls circulation strength. Even $k$, hence the lapse rate, is important when $n$ is low, whereas $k$ loses its importance when the temperature distribution is wider. This result is consistent with results of Tandon et al. (2013) who found that the Hadley cell expansion and jet shift had relatively little sensitivity to the change in the lapse rate. Consequently, the subtropical jet stream intensities are controlled by the broadness of horizontal temperature rather than the vertical lapse rate, with higher values of the jet when the thermal forcing is concentrated to the equator. However, results show that the jet stream position does not show any dependence with $n$ and $k$, except when the temperature distribution is the widest ($n = 3$); in such a case an abrupt change occurs and the maximum of the zonal wind jet is located at mid-latitudes.

*Acknowledgements.* Helpful discussions with Antonio Speranza, Valerio Lucarini and Renato Vitolo are gratefully acknowledged.





NPGD
1, 1621–1655, 2014



## References


Allen, R. J., Sherwood, S. C., Norris, J. R., and Zender, C. S.: Recent Northern Hemisphere tropical expansion primarily driven by black carbon and tropospheric ozone, Nature, 485, 350–354, 2012.

Caballero, R., Pierrehumbert, R. T., and Mitchell, J. L.: Axisymmetric, nearly inviscid circulations in non-condensing radiative-convective atmospheres, Q. J. Roy. Meteorol. Soc., 134, 1269–1285, 2008.

Dima, I. M. and Wallace, J. M.: On the seasonality of the Hadley cell, J. Atmos. Sci., 60, 1522–1527, 2003.

Fang, M. and Tung, K. K.: Time-dependent nonlinear Hadley circulation, J. Atmos. Sci., 56, 1797–1807, 1999.

Fu, Q. and Lin, P.: Poleward shift of subtropical jets inferred from satellite-observed lower stratospheric temperatures, J. Climate, 24, 5597–5603, doi:10.1175/JCLI-D-11-00027.1, 2011.

Fu, Q., Johanson, C. M., Wallace, J. M., and Reichler, T.: Enhanced mid-latitude tropospheric warming in satellite measurements, Science, 312, 1179, 2006.

Gitelman, A. I., Risbey, J. S., Kass, R. E., and Rosen, R. D.: Trends in the surface meridional temperature gradient, Geophys. Res. Lett., 24, 1243–1246, 1997.

Held, I. M. and Hou, A. Y.: Nonlinear axially symmetric circulation in a nearly inviscid atmosphere, J. Atmos. Sci., 37, 515–533, 1980.

Hou, A. Y. and Lindzen, R. S.: The influence of concentrated heating on the Hadley circulation, J. Atmos. Sci., 49, 1233–1241, 1992.

Hu, Y. and Fu, Q.: Observed poleward expansion of the Hadley circulation since 1979, Atmos. Chem. Phys., 7, 5229-5236, doi:10.5194/acp-7-5229-2007, 2007.

Johanson, C. M. and Fu, Q.: Hadley cell widening: model simulations vs. observations, J. Climate, 22, 2713– 2725, 2009.

Kim, H.-K. and Lee, S.: Hadley cell dynamics in a primitive equation model, Part II: Nonaxisymmetric flow, J. Atmos. Sci., 58, 2859–2871, 2001.

Liu, J., Song, M., Hu, Y., and Ren, X.: Changes in the strength and width of the Hadley Circulation since 1871, Clim. Past, 8, 1169–1175, doi:10.5194/cp-8-1169-2012, 2012.

Lu, J., Vecchi, G. A., and Reichler T.: Expansion of the Hadley cell under global warming, Geophys. Res. Lett., 34, L06805, doi:10.1029/2006GL028443, 2007.






NPGD
1, 1621–1655, 2014



Lu, J., Deser, C., and Reichler, T.: Cause of the widening of the tropical belt since 1958, Geophys. Res. Lett., 36, L03803, doi:10.1029/2008GL036076, 2009.
Nguyen, H., Evans, A., Lucas, C., Smith, I., and Timbal, B.: The Hadley circulation in reanalyses: climatology, variability, and change, J. Climate, 26, 3357–3376, 2013.
Polvani, L. M., Waugh, D. W., Correa, G. J. P., and Son, S.-W.: Stratospheric ozone depletion: the main driver of 20th Century atmospheric circulation changes in the Southern Hemisphere, J. Climate, 24, 795–812, doi:10.1175/2010JCLI3772.1, 2011.
Santer, B. D., Thorne, P. W., Haimberger, L., Taylor, K. E., Wigley, T. M. L., Lanzante, J. R., Solomon, S., Free, M., Gleckler, P. J., Jones, P. D., Karl, T. R., Klein, S. A., Mears, C., Nychka, D., Schmidt, G. A., Sherwood, S. C., and Wentz, F. J.: Consistency of modelled and observed temperature trends in the tropical troposphere, Int. J. Climatol., 28, 1703–1722, 2008.
Schaller, N., Cermak, J., Wild, M., and Knutti, R.: The sensitivity of the modeled energy budget and hydrological cycle to $CO_2$ and solar forcing, Earth Syst. Dynam., 4, 253–266, doi:10.5194/esd-4-253-2013, 2013.
Schneider E. K.: Axially symmetric steady-state models of the basic state for instability and climate studies, Part II. Nonlinear calculations, J. Atmos. Sci., 34, 280–296, 1977.
Schneider, E. K. and Lindzen, R. S.: Axially symmetric steady state models of the basic state of instability and climate studies, Part I: Linearized calculations, J. Atmos. Sci., 34, 253–279, 1977.
Seidel, D. J., Fu, Q., Randel, W. J., and Reichler, T. J.: Widening of the tropical belt in a changing climate, Nat. Geosci., 1, 21–24, 2008.
Sherwood, S. C., Meyer, C. L., Allen, R. J., and Titchner, H. A.: Robust tropospheric warming revealed by iteratively homogenized radiosonde data, J. Climate, 21, 5336–5352, 2008.
Staten, P. W., Rutz, J., Reichler, T., and Lu, J.: Breaking down the tropospheric circulation response by forcing, Clim. Dynam., 39, 2361–2375, doi:10.1007/s00382-011-1267-y, 2011.
Strong, C. and Davis, R. E.: Winter jet stream trends over the Northern Hemisphere, Q. J. Roy. Meteorol. Soc., 133, 2109–2115, 2007.
Titchner, H. A., Thorne, P. W., McCarthy, M. P., Tett, S. F. B., Haimberger, L., and Parker, D. E.: Critically reassessing tropospheric temperature trends from radiosondes using realistic validation experiments, J. Climate, 22, 465–485, 2008.
Walker, C. C. and Schneider, T.: Response of idealized Hadley circulations to seasonally varying heating, Geophys. Res. Lett., 32, L06813, doi:10.1029/2004GL022304, 2005.





NPGD
1, 1621–1655, 2014



Walker, C. C. and Schneider, T.: Eddy influences on Hadley circulations: simulations with an idealized GC M, J. Atmos. Sci., 63, 3333–3350, 2006.
Weliser, D. E., Shi, Z., Lanzante, J. R., and Oort, A. H.: The Hadley circulation: assessing NCEP/NCAR reanalysis ans sparse in situ estimates, Clim. Dynam., 15, 719–735, 1999.





NPGD
1, 1621–1655, 2014



**Table 1.** Latitudes (in degrees) of the maximum wind speed for the equinoctial and time-dependent solutions when $k = 1$ as a function of the parameter $n$.

| $n$ | 0.5 | 1 | 1.5 | 2 | 2.5 | 3 |
|---|---|---|---|---|---|---|
| Equinoctial | 27.4 | 28.7 | 27.4 | 26.1 | 28.7 | 47.7 |
| Time dependent | 28.7 | 28.7 | 28.7 | 27.4 | 27.4 | 44.4 |





NPGD
1, 1621–1655, 2014



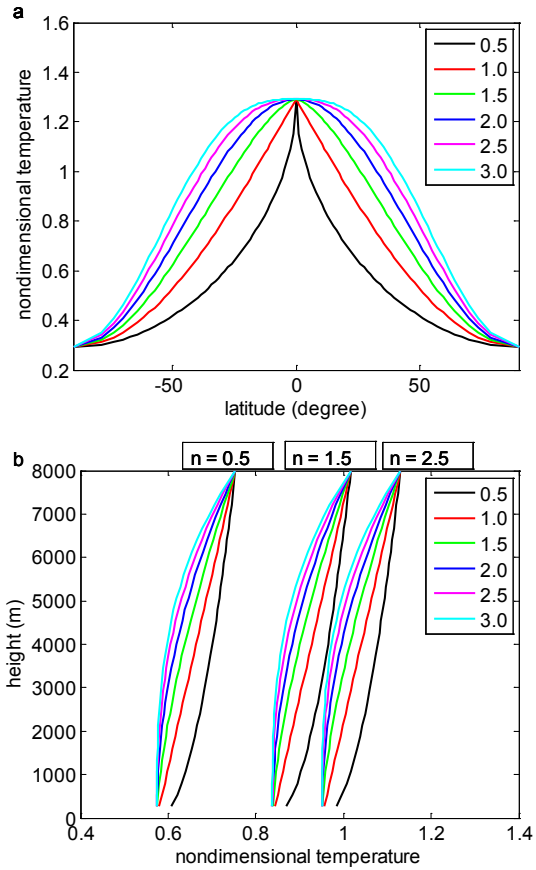


**Figure 1.** Meridional **(a)** and vertical **(b)** mean non-dimensional temperature.





NPGD
1, 1621–1655, 2014

Temperature distribution and Hadley circulation in an axisymmetric model

N. Tartaglione



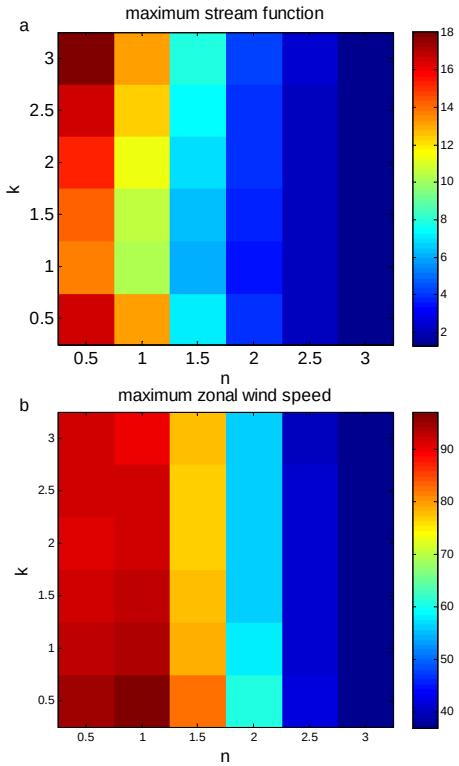


**Figure 2.** Maximum non-dimensional stream function **(a)** and zonal wind speed [ms$^{-1}$] **(b)** as function of parameters $n$ and $k$ for the steady solution.





NPGD
1, 1621–1655, 2014

Temperature distribution and Hadley circulation in an axisymmetric model

N. Tartaglione



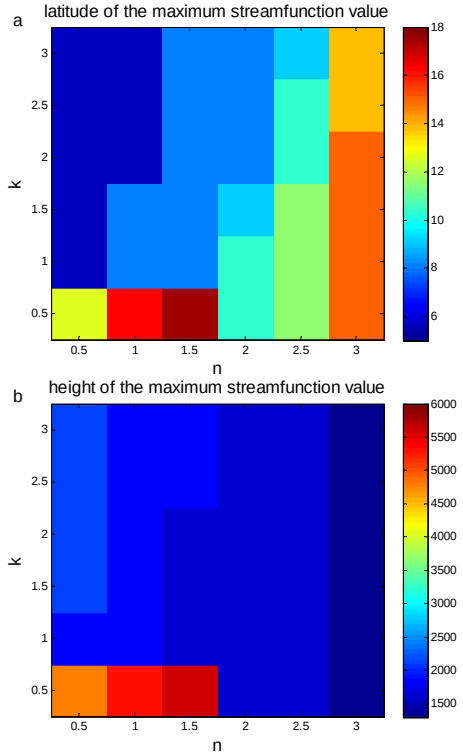


**Figure 3.** Latitude [degree] **(a)** and Height [m] **(b)** of maximum non-dimensional stream function.





NPGD
1, 1621–1655, 2014

Temperature distribution and Hadley circulation in an axisymmetric model

N. Tartaglione



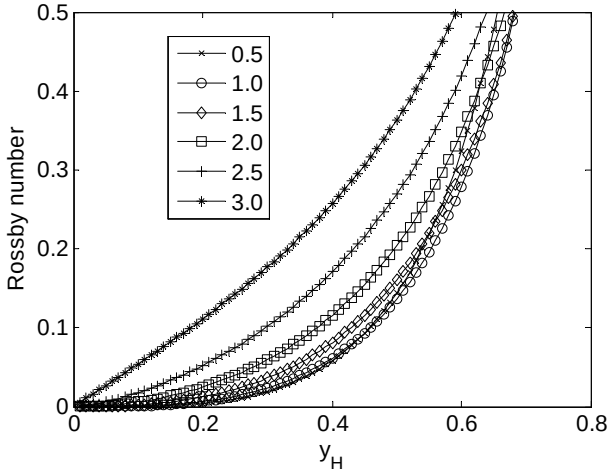


**Figure 4.** Relationship between Rossby number and poleward boundary of the Hadley cell as given by Eq. (10), $y_H = \sin\varphi_H$.





NPGD
1, 1621–1655, 2014

Temperature distribution and Hadley circulation in an axisymmetric model

N. Tartaglione



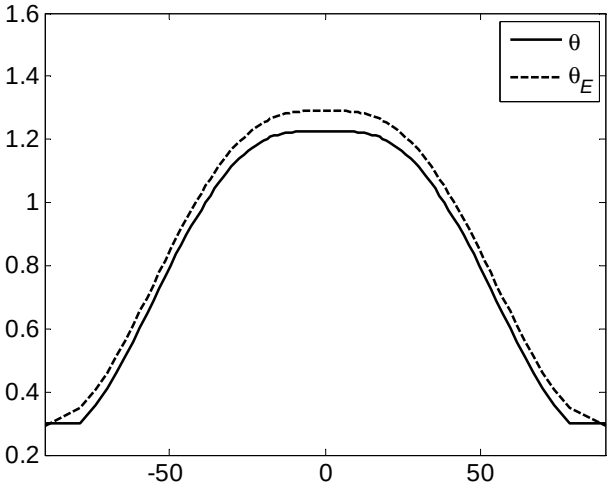


**Figure 5.** Vertically averaged potential temperature for the simulation with $n = k = 3$.





NPGD
1, 1621–1655, 2014

Temperature distribution and Hadley circulation in an axisymmetric model

N. Tartaglione



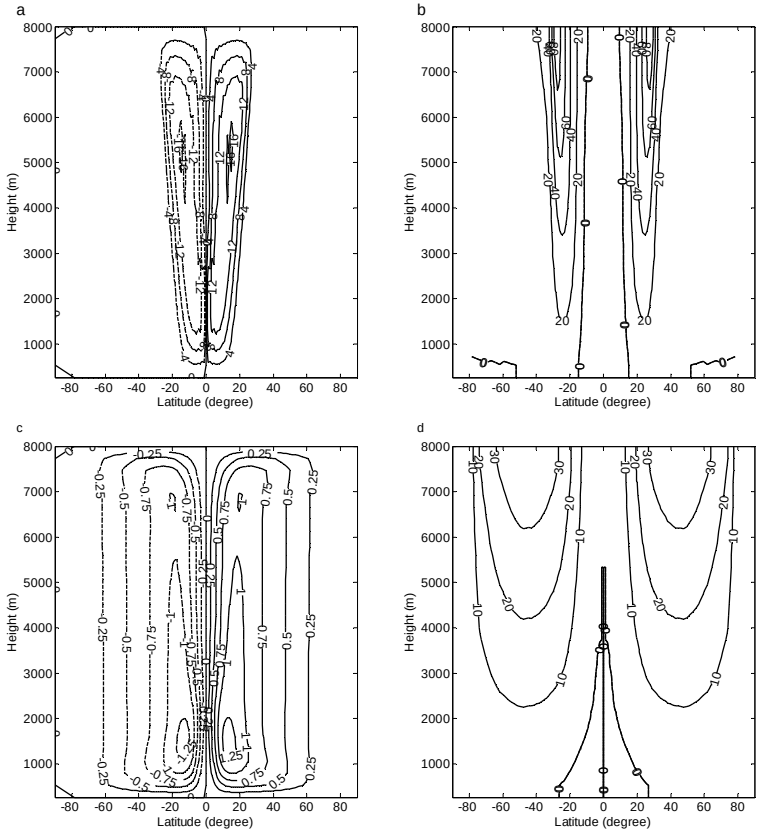


**Figure 6.** Non-dimensional stream function (**a, c**) and zonal wind speed (**b, d**) for the steady cases $n = 0.5$, $k = 0.5$ (upper panels) and $n = 3$, $k = 3$ (lower panels).





NPGD
1, 1621–1655, 2014

Temperature distribution and Hadley circulation in an axisymmetric model

N. Tartaglione



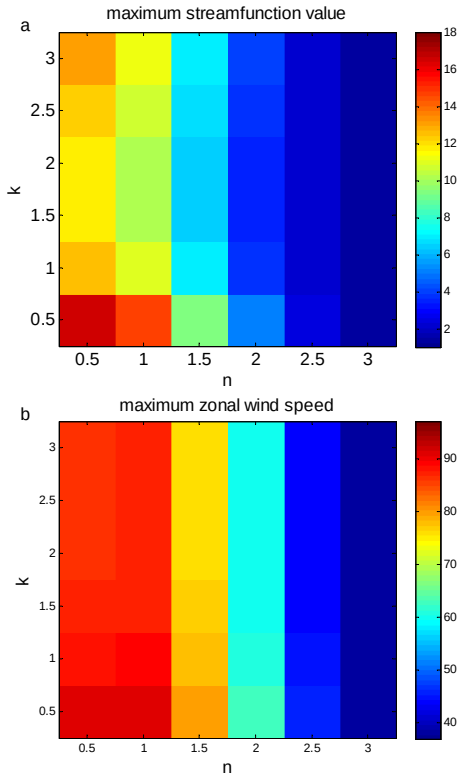


**Figure 7.** Maximum of annually averaged non dimensional stream function **(a)** and zonal wind speed [ms$^{-1}$] **(b)** as function of parameters $n$ and $k$ for the time-dependent simulations.





NPGD
1, 1621–1655, 2014

Temperature distribution and Hadley circulation in an axisymmetric model

N. Tartaglione



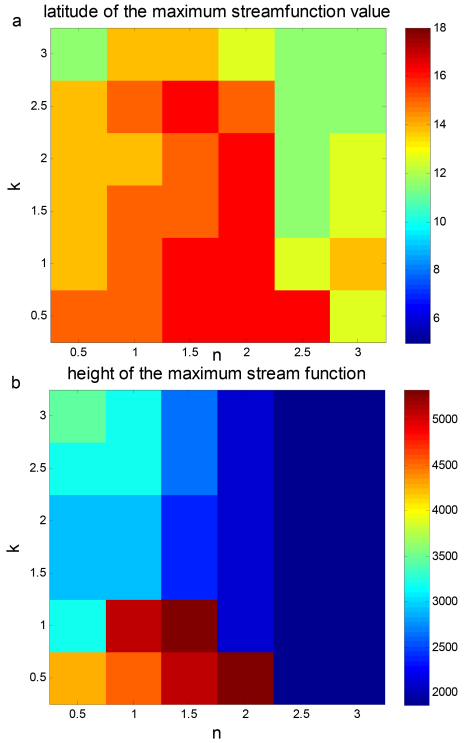


**Figure 8.** Latitude [degree] **(a)** and Height [m] **(b)** of maximum annually averaged non-dimensional stream function for the time-dependent solution.





NPGD
1, 1621–1655, 2014

Temperature distribution and Hadley circulation in an axisymmetric model

N. Tartaglione



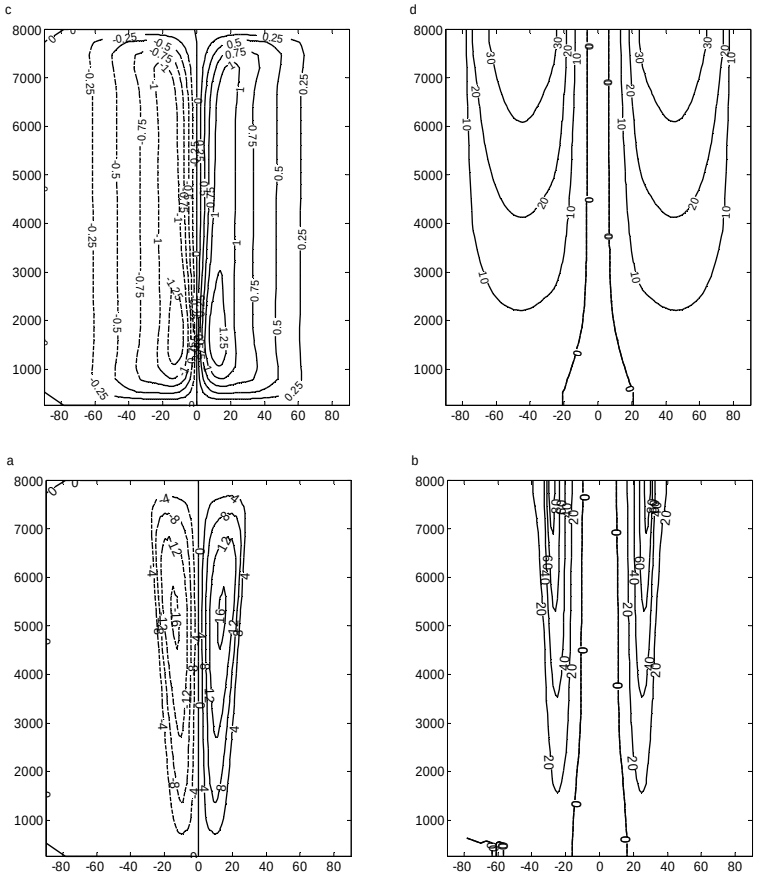


**Figure 9.** Annually averaged non-dimensional stream function (**a, c**) and zonal wind speed (**b, d**) for the steady cases $n = 0.5$, $k = 0.5$ (upper panels) and $n = 3$, $k = 3$ (lower panels).





NPGD
1, 1621–1655, 2014

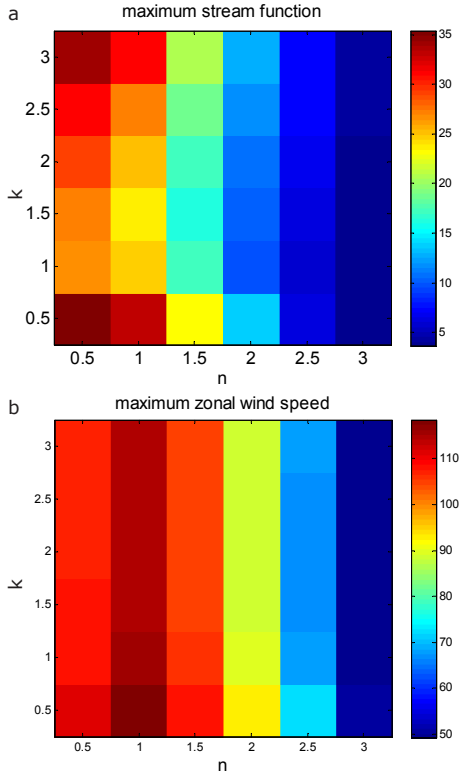


**Figure 10.** Maximum of non-dimensional stream function **(a)** and zonal wind speed [$ms^{-1}$] **(b)** as function of parameters *n* and *k* for the time-dependent simulations.





NPGD
1, 1621–1655, 2014

Temperature distribution and Hadley circulation in an axisymmetric model

N. Tartaglione



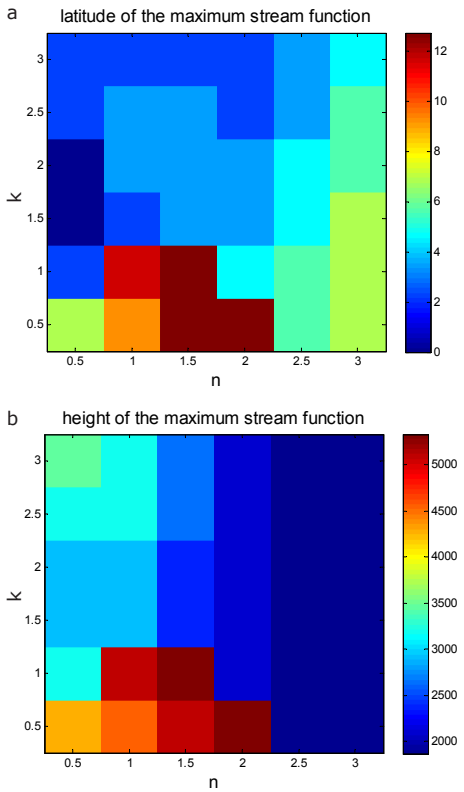


**Figure 11.** Latitude [degree] **(a)** and Height [m] **(b)** of maximum non-dimensional stream function for the time-dependent solution.





NPGD
1, 1621–1655, 2014

Temperature distribution and Hadley circulation in an axisymmetric model

N. Tartaglione



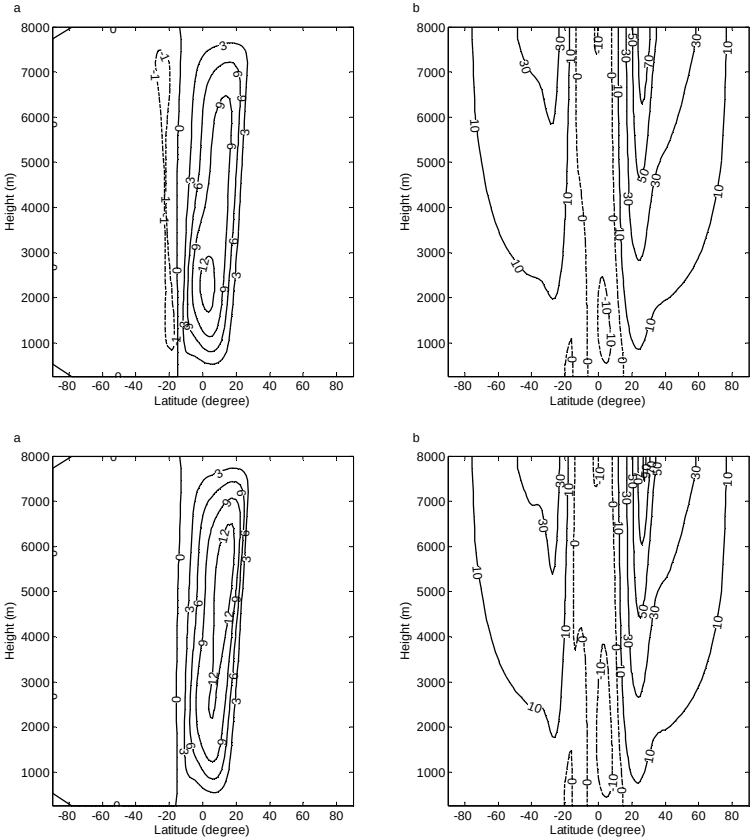


**Figure 12.** Winter circulation, non-dimensional stream function (**a, c**) and zonal wind speed (**b, d**) when $n = 2$, $k = 0.5$ (upper panels) and $n = 2$, $k = 3$ (lower panels) for the time-dependent simulation.





NPGD
1, 1621–1655, 2014

Temperature distribution and Hadley circulation in an axisymmetric model

N. Tartaglione



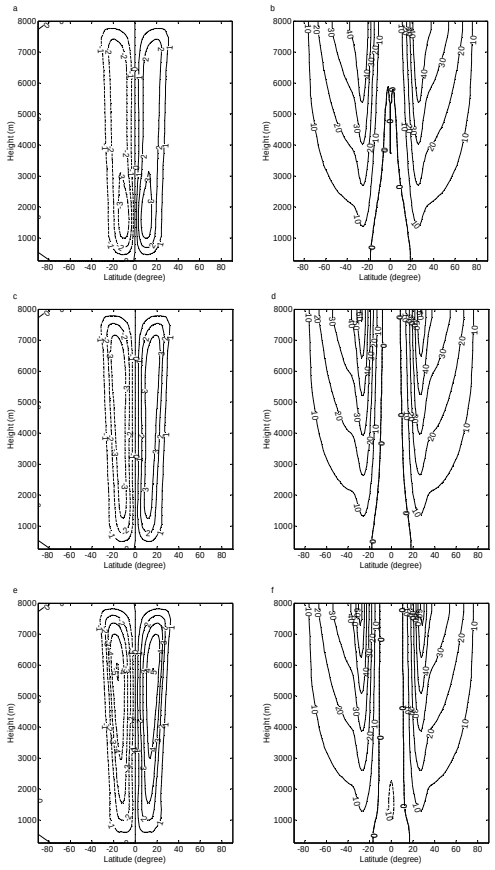


**Figure 13.** Non-dimensional annually averaged stream function **(a, c, e)** and zonal wind speed **(b, d, f)** when $n = 2$ and $k = 1$ for the steady **(a)**, time-dependent **(b)** and with the maximum heating 6° off the equator **(c)**.





NPGD
1, 1621–1655, 2014

Temperature distribution and Hadley circulation in an axisymmetric model

N. Tartaglione